ORIGINAL PAPER

# Quantification and analysis of ecdysis in the hornworm, *Manduca sexta*, using machine vision–based tracking

Alan Shimoide · Ian Kimball · Alba A. Gutierrez ·
Hendra Lim · Ilmi Yoon · John T. Birmingham ·
Rahul Singh · Megumi Fuse

**Abstract** We have developed a machine vision–based method for automatically tracking deformations in the body wall to monitor ecdysis behaviors in the hornworm, *Manduca sexta*. The method utilizes naturally occurring features on the animal's body (spiracles) and is highly accurate (>95 % success in tracking). Moreover, it is robust to unanticipated changes in the animal's position and in lighting, and in the event tracking of specific features is lost, tracking can be reestablished within a few cycles without input from the user. We have paired our tracking technique with electromyography and have also compared our in vivo results to fictive motor patterns recorded from isolated nerve cords. We found no major difference in the cycle periods of contractions during naturally occurring ecdysis compared to ecdysis initiated prematurely through injection of the peptide ecdysis-triggering hormone, and we confirmed that the ecdysis period in vivo is statistically similar to that of the fictive motor pattern.

A. Shimoide · H. Lim · I. Yoon · R. Singh (✉)
Department of Computer Science, San Francisco State University, 1600 Holloway Ave., San Francisco, CA 94132, USA
e-mail: rahul@sfsu.edu

I. Kimball · A. A. Gutierrez · M. Fuse (✉)
Department of Biology, San Francisco State University, 1600 Holloway Ave., San Francisco, CA 94132, USA
e-mail: fuse@sfsu.edu

J. T. Birmingham
Department of Physics, Santa Clara University, 500 El Camino Real, Santa Clara, CA 95053, USA

## Introduction

Understanding an animal's behavior requires that one has the ability to accurately and quantitatively characterize the movements associated with the behavior. Quantitatively documenting a complicated behavior requires a powerful, impartial observer. In this context, video recording an animal's movements followed by algorithmic analysis of the video to make measurements of the observed movements can be a powerful approach. For example, Balch et al. (2001) used color- and movement-based tracking to monitor and analyze the simultaneous positions of hundreds of individual ants living in a colony. In the worm *Caenorhabiditis elegans,* a number of algorithmic techniques were employed to study and characterize shape, motion, and behavior for phenotypic analysis of genetic mutants (Baek et al. 2002; Geng et al. 2004; Buckingham and Sattelle 2008; Cronin et al. 2005; Albrecht and Bargmann 2011; Swierczek et al. 2011). Video-analysis-based methods have also been applied to characterize phenotypes for screening of macroscopic human parasites in high-throughput drug discovery (Singh et al. 2009; Lee et al. 2012; Marcellino et al. 2012). The analysis of such complicated behaviors captured through video requires development of sophisticated algorithms, and these methods have two significant advantages: First, they can be used to accurately quantify complex phenotypes and behaviors. Second, they can be applied at timescales that are either too short or too long for effective human observation. Furthermore, these methods do not require expensive

instrumentation and can often be carried out without restraining the animal's natural behavior.

In this paper, we describe the development of a machine vision–based tracking method to characterize ecdysis, an important behavior in the life of the hornworm *Manduca sexta*. Machine vision denotes the process of video acquisition and automated algorithmic analysis of the video for quantification of the desired behavior. Ecdysis, an essential period at the end of the molt in an insect's life cycle, facilitates shedding of the old cuticle to allow continued growth and development. It is coordinated by hormonal and neural interactions that regulate activation of various underlying central pattern generator networks (Gammie and Truman 1997, 1999; Novicki and Weeks 1993; Zitnan and Adams 2000; reviewed by Ewer and Reynolds 2000). Although a stereotyped behavior, the shedding of the cuticle is fairly complicated and includes a series of distinct patterned motor programs termed pre-ecdysis and ecdysis. Pre-ecdysis involves synchronous rhythmic compressions and relaxations along the entire segmented body wall to loosen the cuticle. Ecdysis itself consists of rhythmic anteriorly directed peristaltic waves that start at the back of the animal and move forward in a wave-like motion, segment by segment (Weeks and Truman 1984; Novicki and Weeks 1993; Zitnan et al. 1999).

Prior strategies for tracking movements in *M. sexta* have included (1) videotaping followed by subjective, labor-intensive frame-by-frame assessment of movements (Weeks and Truman 1984) and (2) attachment of fluorescent external markers to the body wall to monitor locomotion (Mezoff et al. 2004). Both approaches were subject to limitations. In the first study, the cuticle was removed when videotaping the ecdysis behaviors because segment divisions, which were used for visualizing body movements, were occluded as the cuticle was shed. This also eliminated sensory feedback related to removal of the cuticle, and the authors noted that ecdysis was prolonged when the cuticle was removed, suggesting that cuticle removal may have modified the behavior itself (Weeks and Truman 1984). Fluorescent external markers were successfully used for assessing general locomotion (Mezoff et al. 2004), but would be lost or obscured if used for monitoring ecdysis, as the cuticle was shed over the course of the behavior.

In our study, we monitored deformations in the body wall by tracking naturally occurring markers or fiducials on the animal's body. These markers were the animal's spiracles, which are the external tracheal apertures located on each segment of the body. In developing our tracking tool we considered (1) the robustness of the program in handling extensive video footage with unconstrained lighting and animal postures, and motion patterns of varying complexity, (2) accuracy of tracking, and (3) accuracy of

automated data analysis while allowing the user to control critical parameters in the analysis process if desired. In this paper we demonstrate that our technique successfully provides a quantitative description of in vivo ecdysis behaviors, even under non-ideal conditions. We also paired video tracking with electromyographic (EMG) recordings and compared our data to electrophysiological recordings from the isolated nervous system. We found that behaviors in animals ecdysing naturally were similar to those undergoing precocious ecdysis after injection with ecdysis-triggering hormone (ETH), and we confirmed that sensory feedback does not play a major role in shaping the basic ecdysis motor program.

## Materials and methods

### Animals

Larvae of the tobacco hornworm *M. sexta* (Lepidoptera: Sphingidae, L.) were reared in isolation in a 17:7-h light:dark photoperiod coupled to a thermoperiod of 27:25 °C with 50–60 % relative humidity (Wells et al. 2006). They were fed an artificial diet (MP Biomedicals, Santa Ana, CA, USA) based on the methods of Bell and Joachim (1976). Pharate fifth-instar larvae were timed to the "air-filled brown mandible" stage, a developmental marker reached approximately 5 h before ecdysis to the fifth instar (Copenhaver and Truman 1982; Schwartz and Truman 1983). A total of 51 larvae were used in this project, and groups of 4–12 larvae were used in any experiment, as described in the figure legends.

### Initiation of ecdysis

Larval *M. sexta* were either induced to undergo precocious ecdysis by injection of the peptide ETH or were allowed to undergo naturally occurring ecdysis. Then 1–2 h after timing to the "air-filled brown mandible" stage, animals to be treated with ETH were anaesthetized on ice for 15 min and immediately prepared for recordings. Approximately 10 min after the start of recordings, animals were injected in the terminal abdominal segment with 10 µl of $2 \times 10^{-5}$ M ETH (200 pmol ETH per animal) using a 10-µl syringe (Hamilton Company, Reno, NV, USA) as previously described (Fuse and Truman 2002).

ETH was synthesized at 95 % purity (Peptron Inc., Daejeon, S. Korea and SynBioSci Corp., Livermore, CA, USA) and stored in $10^{-2}$ M aliquots in modified Miyazaki's saline (Trimmer and Weeks 1989) at −20 °C until needed for experiments. Intact larvae were injected with ETH diluted further in modified Weever's saline (Trimmer

and Weeks 1989), and isolated CNS preparations were incubated in ETH diluted in Miyazaki's saline.

## Video tracking

Video tracking was composed of four steps: (1) digital video capture and storage of the footage as a series of images (hereafter called "frames") in the QuickTime format, (2) image pre-processing to identify features on the larva, including body wall and spiracles, (3) tracking of the identified features (spiracles) and recording their $(x, y)$ coordinates, and (4) automated analysis of the data.

### Videotaping and video conversion

Prior to videotaping, animals were positioned on a black stage. To aid in calibration during image tracking, a ruler with 1 cm increments was placed immediately next to the animal's feet. After visual confirmation of the start of pre-ecdysis, recording with a video camera (Sony DCR-SR40 or TRV740 Digital-8 Camcorder, with a Raynox DCR-150 MacroScan close-up conversion lens and RA5237 lens adapter) was initiated. In experiments in which EMG recordings were performed simultaneously, the start of video recording was marked on the EMG trace as well, to allow the time courses of the two recordings to be synchronized. The video recording was stopped when the EMG trace was no longer readable, when ecdysis had ceased, or when 15 min had passed. Video was imported to a computer, and the movie was converted into a sequence of images (jpeg or png format), where each image corresponded to a frame.

### Machine vision–based segmentation and tracking

We used machine vision for segmenting and tracking the larva and analyzing its motion during ecdysis. In the context of image analysis, segmentation refers to the identification of the object of interest (in our case the larva) within the scene. In this section, we describe the key parts of this method.

For purposes of segmentation and subsequent tracking, the body of the larva was modeled using *regions of interest* (ROI) and relationships defined between ROIs. Specifically, the body and spiracles (Fig. 1a, b; black arrowheads) of the hornworm were defined as ROIs, and a hierarchical parent–child relationship was established with the body being the parent ROI (Fig. 2a, c; red boxes) and each spiracle being a child ROI (Fig. 2c, blue boxes). This hierarchy captured the natural constraint that a child ROI could only be located inside the parent ROI.

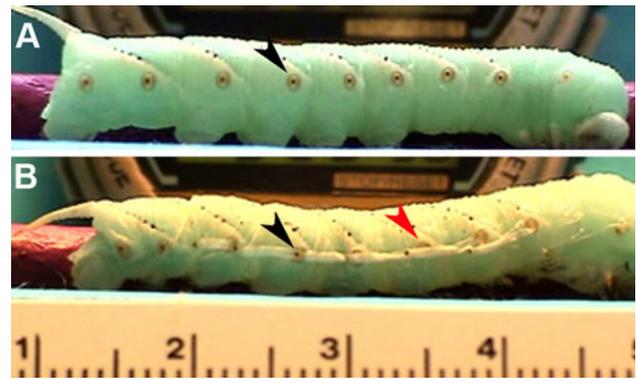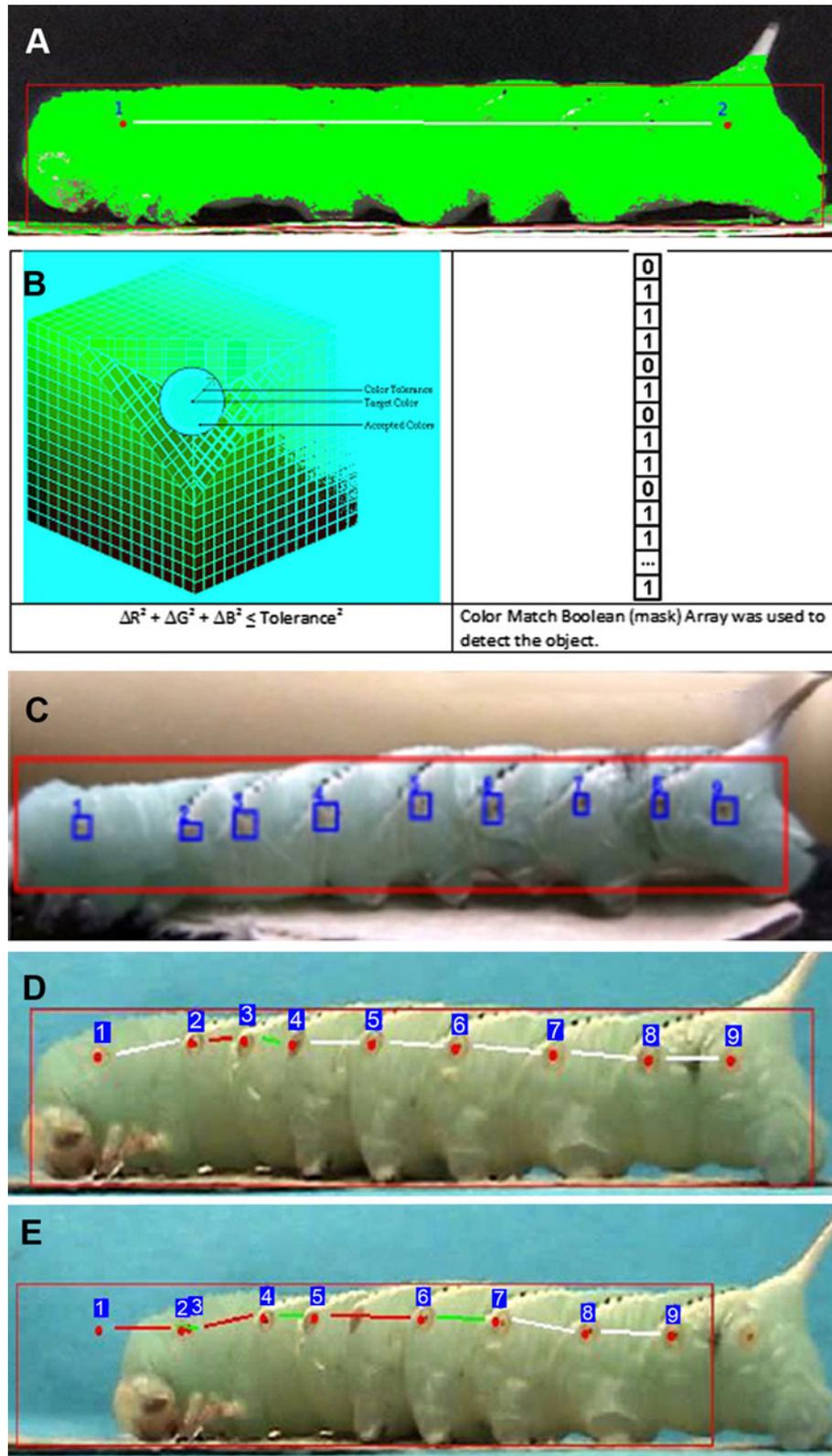Next, an algorithmic approach based on color-constrained region matching was used to simultaneously



**Fig. 1** Two frames from video clips of *M. sexta* showing a side profile with head at the *right*. **a** *M. sexta* prior to the onset of ecdysis. The *black arrowhead* shows the location of a spiracle in the fifth segment. **b** *M. sexta* undergoing ecdysis. The spiracles (*arrowheads*) are tracked and may remain highly visible (*black*) during ecdysis or may be partially covered by cuticle emerging from the more anterior spiracles (*red*). Measurements on the ruler are in centimeters

segment the body of the hornworm from the background and track it across the frames constituting the video (Fig. 2b). For each video, this process was initiated through an initial user–data interaction step where the user selected the parent ROI corresponding to the body of the animal (Fig. 2a) (henceforth called body-ROI) and the child ROIs, or spiracles (henceforth called spiracle-ROIs). The area surrounding the body-ROI was thus identified to be the background. The pixels in the body and the background were analyzed in terms of their color characteristics, and regions of the color space corresponding to the body and background were identified as described in our earlier work (Shimoide et al. 2005). An illustration is provided in Fig. 2b.

Once the color characteristics of the regions corresponding to the larva and the background were established, binary image segments were matched and extracted by color-constrained minimization of the mean absolute distance between pixels belonging to regions in successive frames of the video. For example, in a particular frame, pixels representing the animal body were found by searching within a specific distance from the last known location of similar pixels in the animal body in the previous frame. Similarity of pixels during this process was defined in terms of their color. This method was based on the observation that the motion of the animal occurred in small increments between frames and that large spatial displacements were rare. This idea was implemented by using a bivariate probability density function (PDF) to weight the distribution of pixels in a frame. Pixels with similar color that were close to the last known location of the larva (in the previous frame) were assigned the highest probabilities of belonging to the foreground object, while pixels far from the last known location were assigned low probabilities. In

**A**

**B**

$$\Delta R^2 + \Delta G^2 + \Delta B^2 \leq Tolerance^2$$

Color Tolerance
Target Color
Accepted Colors

Color Match Boolean (mask) Array was used to detect the object.

**C**

**D**

**E**

the case where pixels with similar color were not found in the search area, the search area was expanded. This approach allowed the program to begin by searching only a small area around the last known position of the larva to find a match in the subsequent frame and expand this search area dynamically only when required.

◄ **Fig. 2** Identifying ROI in images of *M. sexta*. **a** *M. sexta* is presented with head to the *left*, with a bounding *box* identified by the user (*red*), and no color discrimination. The *red box* represents the body-ROI. *Points 1* and *2* in *red* represent the anterior- and posterior-most spiracles, respectively. **b** The method of finding the group of pixels that identify the body is illustrated. Objects are selected using the 3D color histogram. The *left* image shows the 3D color space as *red*, *green*, and *blue*. These *colors* can also be represented as 24-bit arrays as seen in the *right* image where the first eight bits are used for the *red color*, the next eight bits for the *green color*, and the last eight bits for the *blue color*, to constitute one pixel color. As the three axes of the histogram are independent of each other, they can be represented in 3D space and slight variations in either *red*, *green,* or *blue* in quantity are allowed, as they can be considered similar *colors*. The *right* image shows masking in the bits, allowing the *left* image to be determined in bit level computation quickly. **c** The user's initial input for tracking video clips includes a bounding *box* for the body-ROI (*red*) and outlines of spiracles as child spiracle-ROIs (*blue*). Spiracles are incrementally numbered by their positions from anterior (*left*) to posterior (*right*), or head to tail. **d** Tracking is turned on so the viewer can see whether spiracles and body are accurately identified. The *red box* outlines the body-ROI, and *red dots* represent consecutively numbered spiracle-ROIs. *White lines* represent no movement between two spiracles compared to the previous frame, *green lines* represent contractions (shortened distance), and *red lines* represent relaxations (lengthened distance). The figure is truncated slightly in this example for visual clarity. **e** An instance in which there has been a brief loss of body and spiracle-ROI tracking. The image has been slightly reduced compared to **d** to allow all components of tracking to be seen. The brief loss of body-ROI is generally corrected for automatically

To complete the foreground object identification, the color-matching pixels were clustered by spatial contiguity using a flood-fill algorithm (Jain et al. 1995). Each cluster was next assigned a score, which reflected the extent to which its pixels were close to the position of the animal in the previous frame, and the cluster with the largest probability was selected to represent the animal. Once the animal was identified, its shape and position were characterized using the first-order moments of the pixels belonging to the corresponding cluster. In a frame, once the body of the larva was identified, the constituent spiracle-ROIs were also identified using the same approach that had been used to identify the animal's body.

Electromyography (EMG)

Animals were anesthetized on ice for 10–15 min, approximately 2 h prior to expected ecdysis, and prior to electrode insertion. Each animal was then placed on its left side, and in a manner similar to that described by Dominick and Truman (1986), a pair of electrodes composed of fine-gauge 0.003″ enamel-coated copper magnet wire was inserted into a particular segment under its cuticle (Fig. 4a) approximately 3 mm apart. The enamel had been removed from the wire tips leaving a small area of bare wire, and the two leads were inserted into internal longitudinal muscles to record activity from both the tergosternal and

intersegmental muscles (Mesce and Truman 1988). The leads were cemented in place with VetBond adhesive (3 M, St. Paul, MN, USA), and a ground wire was inserted through the cuticle of the posterior proleg. After all leads were inserted, the larva was able to move freely.

The signal was amplified and filtered by a differential AC amplifier (Model 1700, A-M Systems, Carlsborg, WA, USA) and viewed, stored, and analyzed using Spike 2 software (CED Inc., Cambridge, England). In our analysis of EMG recordings, we focused on the cycle period, where we defined a cycle as being a burst plus the following interburst interval. When EMG recordings were collected alone, pairs of recording electrodes were inserted into two adjacent segments to allow simultaneous recordings to be made from the two segments (Fig. 4a). When EMG recordings were paired with videography, EMG was recorded from a pair of electrodes in a single segment (*n*th segment), while spiracles from the *n*th and $(n + 1)$th segments were tracked (Fig. 5a). During all recordings, contractions were marked on the computer by the user to ensure that the recorded EMG cycles of activity paralleled contraction cycles.

Extracellular recordings from the isolated CNS

Animals were anesthetized as described above prior to dissection of the ventral nerve cord and brain. A dorsal incision was made from the anterior to the posterior end of the larva, and the cuticle was pinned open on a Sylgard-184-coated dish (Dow Corning, Midland, MI). The nerve cord was dissected out in Weever's saline and then transferred to 1 ml of Miyazaki's saline in a separate dish reserved for extracellular recordings. Glass suction electrodes were used to make recordings from dorsolateral nerve branches of consecutive abdominal ganglia (typically ganglia 4 and 5 or 5 and 6), during which preparations were maintained at 26 °C. The preparations were then bathed in 1 μM ETH in Miyazaki's saline approximately 10 min after commencing extracellular recordings, as previously described (Ewer et al. 1997; Wells et al. 2006). Fictive pre-ecdysis and ecdysis motor patterns were amplified and filtered by the A-M Systems differential AC amplifier (Model 1700, A-M Systems, Carlsborg, WA) and viewed, stored, and analyzed using Spike 2 software (CED Inc., Irving, TX).

## Results

Tracking ROIs: accuracy of tracking
with and without noise

To gauge the accuracy of the "Feature Tracking" algorithm, the locations of the spiracles were tracked in video clips for

nine animals using a Java implementation of the algorithm. In doing so, an observer could visually monitor how well each spiracle was tracked by determining whether or not a red dot was associated with each spiracle in any given frame (compare Fig. 2d, e). Misplacement of one or more features (the red dot no longer overlaying the spiracle; Fig. 2e "1") was defined as an error, but this error was often corrected automatically by the tracking algorithm itself. By monitoring the presence or absence of the red dots corresponding to the nine spiracles, we rapidly analyzed and assessed the accuracy of tracking of multiple features. Tracking accuracy was tested on three animals from three categories of video clips each: videos with significant noise, videos in which the cuticle partially or wholly occluded the spiracles (Fig. 1b; red arrowhead), and videos with no significant noise. Significant noise included changes in body position when the camera was moved radically or when the organism rolled over or was manipulated by the researcher, or when lighting changed in the video (compare lighting of Fig. 1a, b). Videos in which spiracles were blocked did not generally have other visual disruptions. Videos without significant noise did not show changes in lighting or movement, nor were the spiracles hidden during ecdysis.

### Accuracy of tracking ROIs: videos with significant noise

Out of 7,350 frames analyzed, there were 1,890 frames with significant noise. Out of the 66,150 features (7,350 frames with nine spiracles tracked in a frame), there were about 3,000 features (2,100 frames with one or two errors) with tracking errors. This resulted in a 95.5 % success rate at a feature level. If a frame contained features that were associated with low confidence values, then these specific features and the corresponding frames were marked as low confidence data points. The user could select to omit these features or the entire frame if, for instance, the frame contained multiple low-confidence features. Alternatively, the user could manually redefine the animal's body outline as well as spiracle locations frame by frame through the user interface.

### Accuracy of tracking ROIs: cuticle partially or wholly occluded by the spiracles

Out of 80,460 features analyzed, there were about 3,500 features with tracking errors due to the cuticle partially or wholly covering the spiracle (1,860 frames with errors in tracking the location of two spiracles or fewer). This resulted in a 95.4 % success rate in tracking these videos.

### Accuracy of tracking ROIs: videos without significant noise

Out of approximately 53,000 tracked features (5,880 frames with nine spiracles tracked in each frame), there

were about 150 features for which tracking errors were observed. That is, 99.8 % of the features were tracked successfully. Most of the tracking errors were due to errors in tracking the location of only one or two spiracles in a given frame and in general could be handled as outliers since the tracking of these spiracles in nearby frames tended to be accurate. Such errors were automatically corrected within a few frames.

In summary, when considering features in all three categories, the success rate was 96.7 % (6,650 errors out of 199,610 features). Even when frames were severely noisy or when animals moved out of the bounding box frame (e.g., Fig. 2e) or fell over (see section below), the algorithm was able to automatically reestablish tracking within a few cycles without interference from the user.

### Automated analysis of tracked data

With successful tracking, the distances between all pairs of consecutive spiracles over time could be calculated (Fig. 3); this was represented as $n - 1$ individual time series, where $n$ was equal to the number of spiracles tracked (typically 9; Fig. 3a). Because adjacent spiracles moved closer during contractions and further apart when corresponding muscles were relaxed, plots of interspiracle movements showed a cyclic series of peaks and troughs, which were identified by automated analysis (Fig. 3b). Typically, a default threshold was used for identifying peaks and troughs, although our program allowed the user to choose the value of the threshold as well. The choice for the default was made after running tests on a variety of threshold values. We observed that threshold values higher than the default often resulted in the misidentification of multiple contractions as single contractions, while lower threshold values often led to the misidentification of a bumpy single contraction as multiple separate contractions. Even with an optimum threshold, however, errors could occur, and so a visualization tool provided the user with the ability to see all identified waves. Each cycle was identified by a bounding box (Fig. 3b), which could be altered manually by the user to correct questionable contractions that might have been misidentified in the automated approach. Most cycles were accurately identified (e.g., Fig. 3b; blue arrowheads). Occasionally, two cycles were misidentified as one (e.g., Fig. 3b; pink arrowheads), most typically if one of the two cycles was small in amplitude.

We verified that peaks and troughs were detected accurately by comparing cycle periods from the automated data to those we determined by manually correcting for all misidentified peaks (removing or adjusting all questionable bounding boxes) using the visualization tool. Analysis of variance indicated that there were no significant differences in contraction cycle periods measured automatically or
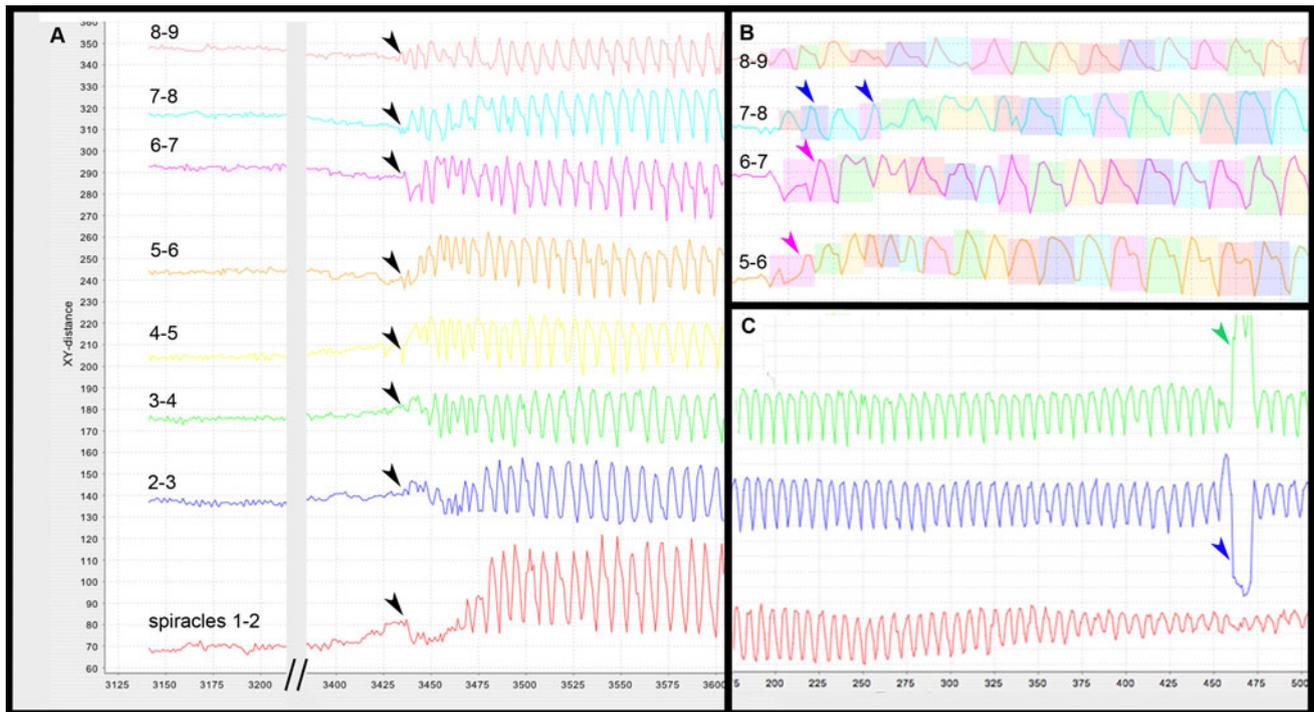
**Fig. 3** Representative windows from the "Feature Tracking and Automated Analysis" program. **a** Nine spiracles were tracked simultaneously for approximately 500 s. The movements of spiracles between two adjoining segments are plotted and labeled, arbitrarily offset from one another for clarity. The *y* axis represents the pixel distance in the image plane between spiracles. The *x*-axis plots the time (in seconds) after the commencement of video recording. The initial flat portion of the data (*before* the *black arrowheads*) corresponds to pre-ecdysis, which is not tracked by this program, while the *oscillating waves* represent contractions of the segments of the body during ecdysis. **b** Automated processing of four segments from **a**, where each cycle is identified by automated analysis and outlined by a *colored* bounding *box*. The *blue arrowheads* represent examples of correctly identified cycles. The *pink arrowheads* indicate examples where two cycles were misidentified as one cycle. **c** Three spiracles were tracked from a different video clip until the animal fell over. The *blue* and *green arrowheads* identify the point where tracking was lost after the animal fell and then reidentified

after manual correction, for 8 min of recorded ecdysis behavior (data not shown; $p = 0.11$, $n = 6$). These results confirmed that our automated approach accurately identified contractions across an entire data set using a single threshold value. When the animal fell over, resulting in a big shift in position (Fig. 3c; blue and green arrowheads), the program rapidly and automatically reidentified the fiducials and carried on tracking.

### Observations of ecdysis in *M. sexta*

#### Video tracking correlates with EMG activity

Because ecdysis EMG activity was previously described during adult eclosion and ascribed to specific muscle groups (intersegmental and tergosternal; Kammer and Kinnamon 1977; Mesce and Truman 1988), we inserted electrodes in larval muscle and recorded in neighboring segments in animals in which ecdysis was initiated via subsequent ETH injection. We measured EMG bursts that corresponded directly to observed pre-ecdysis and ecdysis contractions (Fig. 4). Pre-ecdysis patterns consisted of higher-frequency, small potentials that occurred synchronously between two segments (Fig. 4b). Behaviorally, these corresponded to the dorsoventral contractions that we observed to be occurring simultaneously in each segment. The EMG recordings during the transition period consisted of tonic activity, which we observed visually as weak and arrhythmic uncoordinated dorsoventral and anterior–posterior contractions. Ecdysis patterns corresponded to phase-shifted bursts of EMG activity in adjacent segments (Fig. 4a) and consisted of larger potentials than those seen during pre-ecdysis (Fig. 4b). After characterizing the EMG recordings from adjacent segments, we made paired recordings of EMG and video tracking for larvae undergoing ecdysis (Fig. 5). Because the EMG profile differed so greatly between pre-ecdysis and ecdysis patterns, simultaneous recordings from multiple segments were not necessary to distinguish between pre-ecdysis and ecdysis rhythms, and so we used a single pairs of EMG electrodes. Figure 5a shows the EMG and video tracking recordings during the onset of the ecdysis motor program monitored in segments 4 and 5. Tracking data paralleled EMG activity. Figure 5b summarizes the results of four experiments and
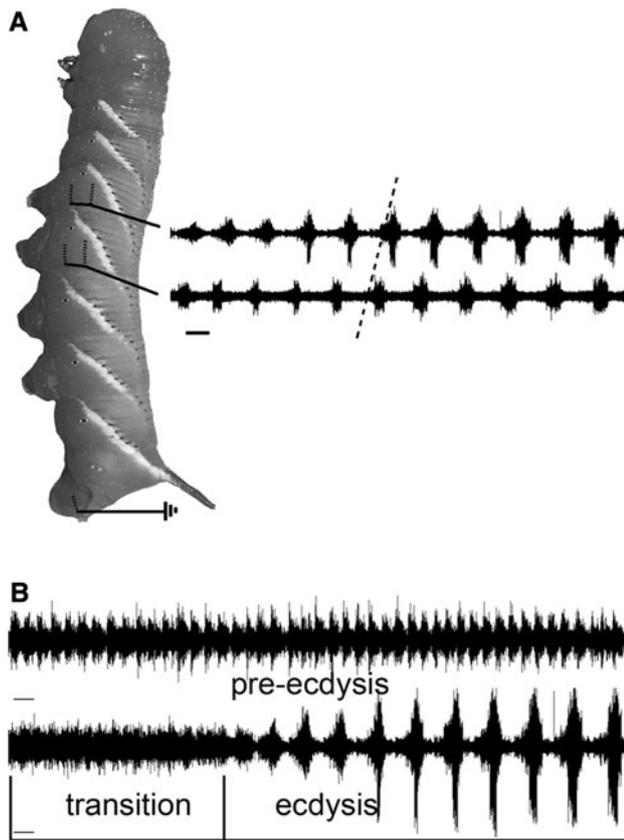
**Fig. 4** Electromyographic (EMG) recordings of muscle activity during ecdysis in *M. sexta*. **a** At *left*, diagram of vertically arranged larva, with head at the *top*. *Thick black lines* indicate the site where two pairs of electrodes were inserted into two consecutive segments (3 and 4 in this example) for EMG recordings. The *dashes* show where the electrodes were inserted through the cuticle. A *third line* indicates the ground wire that was inserted in the proleg of segment 8 at the posterior end of the animal. At *right*, the traces show simultaneous EMG recordings of ecdysis from the third and fourth segments. Bursting in the third segment lags that of the fourth segment, as noted by the *dashed line*. **b** An EMG trace recorded from segment 5 after injection of ETH, showing pre-ecdysis (started 7 min after injection), the transition to ecdysis, and ecdysis (started approximately 42 min after injection of ETH). *Scale bar* in all panels = 10 s

shows that the average cycle period, as measured using either technique, increased from an initial value of 12 s to approximately 20 s over the first ten cycles. Cycle period was not found to be significantly different ($p = 0.41$) between the two techniques.

### ETH-induced ecdysis behaviors are similar to natural behaviors

We used video tracking to compare ETH-induced ecdysis to natural ecdysis (Fig. 6a) and found no significant differences in the ecdysis cycle periods between the two methods ($p = 0.54$) during the 6–10 min that it typically
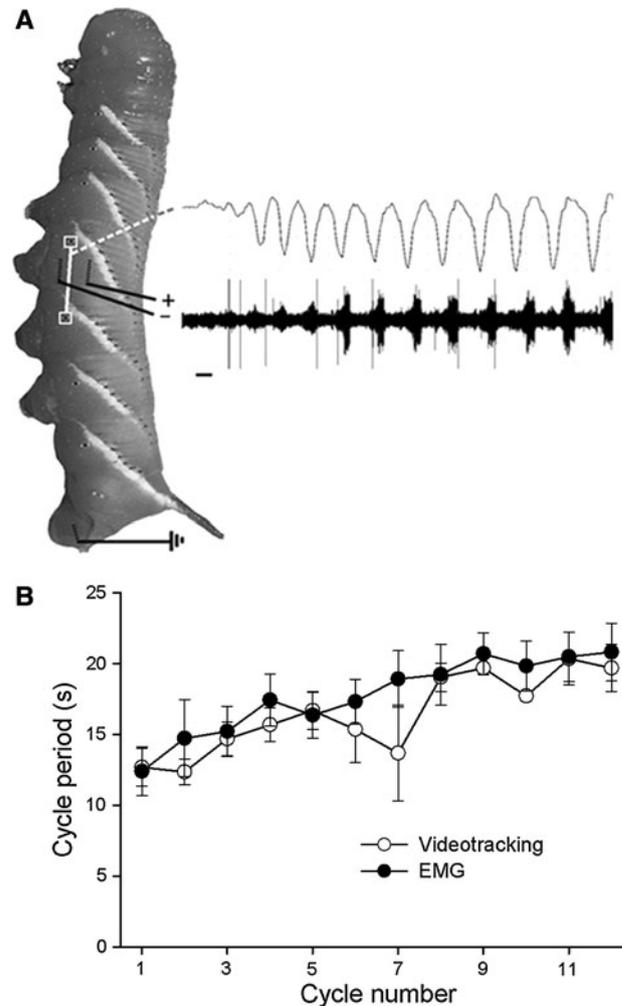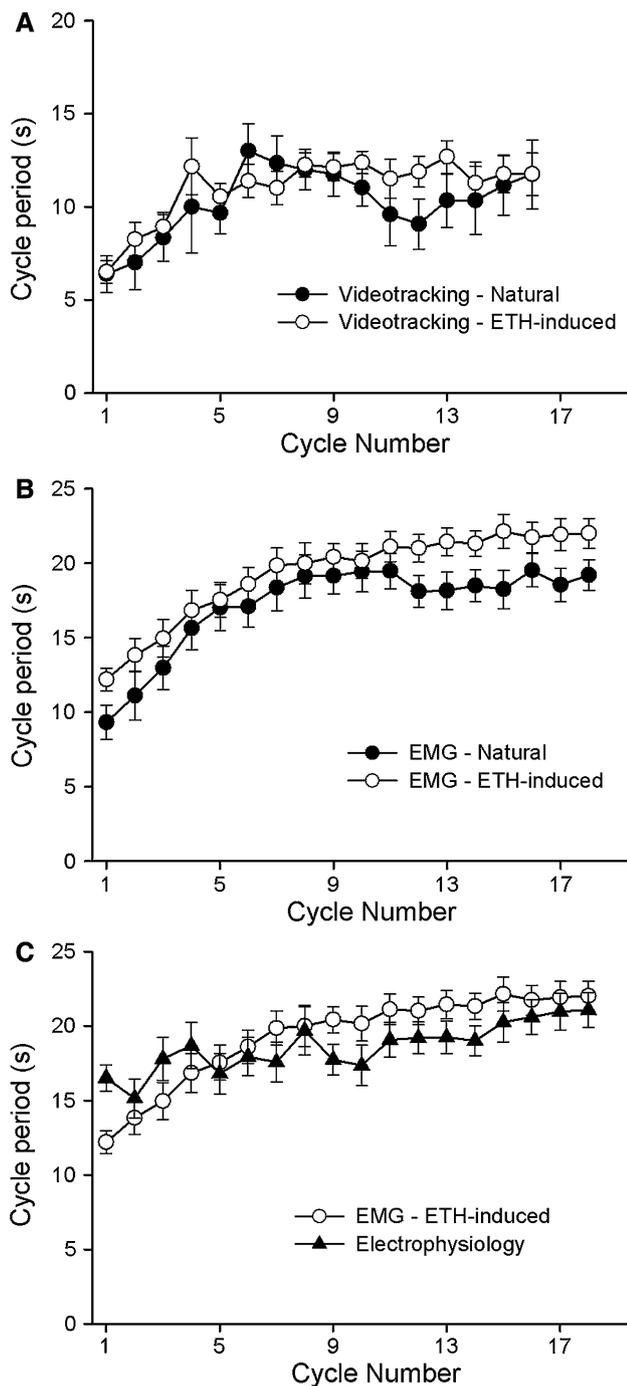
**Fig. 5** Recordings of muscle activity and movements during ecdysis in *M. sexta*. **a** At *left*, diagram of vertically arranged larva, with head at the *top*. *Thick black lines* indicate the site where individual electrodes were inserted for EMG recordings in segment 4. The *dashes* show where the electrodes were inserted through the cuticle. The ground electrode was inserted at the posterior end. *White boxes* outline the spiracles from segments 4 and 5 that were monitored by video tracking, and the *solid white line* indicates the distance between them at that point. At *right*, the *top* trace shows tracking of the distance between spiracles 4 and 5 as a function of time during ecdysis, and the *bottom* trace shows simultaneous EMG recordings from segment 4. *Scale bar* 10 s. **b** Cycle period as a function of the cycle number from simultaneous video tracking (*open circles*) and EMG recordings (*filled circles*) of ecdysis behaviors ($n = 4$). Recordings were made at 26 °C. Two-way analysis of variance revealed no significant differences between the treatments ($p = 0.41$)

took to fully shed the cuticle. During this time, our video tracking measurements showed that the cycle period progressively increased over time in a manner parallel to that seen in Fig. 5b. EMG recordings under natural and ETH-induced conditions (Fig. 6b) produced similar results, where cycle periods were not significantly different from each other ($p = 0.15$).

**Fig. 6** Cycle period as a function of cycle number from video-tracked data. Animals were videotaped undergoing "natural" ecdysis (*filled circles*) or "ETH-induced" ecdysis (*open circles*). **a** Recordings were made at 21 °C for animals undergoing "natural" ecdysis ($n = 8$) or "ETH-induced" ecdysis ($n = 8$). Two-way analysis of variance revealed no significant differences between groups ($p = 0.54$). Recordings of ETH-induced ecdysis made at 26 °C showed a range of burst periods from 9 to 18 s ($n = 3$, data not shown), indicating that placement of EMG electrodes was not the cause of the increased burst period. Thus, the differences in initial periods were attributed to the different recording temperatures for the two experiments (21 vs. 26 °C) since paired video tracking and EMG recordings had identical periods over the course of the behaviors (Fig. 5b; 26 °C). **b** EMG activity was recorded under "natural" ($n = 6$) or "ETH-induced" ($n = 12$) conditions. Recordings were made at 26 °C. Two-way analysis of variance revealed no significant differences between groups ($p = 0.15$). **c** Cycle period as a function of cycle number from EMG recordings taken from (**b** *open circles*) and fictive motor patterns from an isolated nerve preparation (*filled triangles*; $n = 9$). Recordings were made at 26 °C. After the first cycle, there were no significant differences between methods overall ($p = 0.61$)

providing exogenous ETH. As with video tracking and EMG data, the cycle periods of the fictive motor programs increased toward the end of the recording, but other than the first cycle ($p = 0.018$), there were no significant differences between the EMG recordings and extracellular electrophysiology of isolated nerve cords ($p = 0.61$).

## Discussion

The primary goals of this project were to develop a novel tool for extracting quantitative data from video recordings of whole-animal behaviors and to compare our findings to the limited amount of data obtained from manually analyzed video footage (Weeks and Truman 1984) and from data collected using more well-established methods (e.g., electromyography (Mesce and Truman 1988) and electrophysiology (Weeks and Truman 1984; Gammie and Truman 1997)). Our video tracking technique proved a robust and reliable method for monitoring ecdysis, producing quantitative results that were consistent with those that we obtained using EMG. Most importantly, the use of spiracles as tracking fiducials, in contrast to the approach taken in a previous investigation (Weeks and Truman 1984), allowed observation of ecdysis behaviors in an entirely intact animal without the need to remove the cuticle. In spite of the differences in techniques, by and large, the results from our automated investigation were consistent with the previous studies (Weeks and Truman 1984; Mesce and Truman 1988). Plots of interspiracle movement showed a cyclic series of peaks and troughs, representative of relaxation and contraction phases with a gradual lengthening of the period over the duration of the behavior. As with Weeks

*In vitro fictive ecdysis motor patterns are similar to ecdysis behaviors*

Figure 6c summarizes measurements of the ecdysis cycle period determined from EMG recordings of intact animals (data taken from Fig. 5b) and of nerve cord preparations. Different animals were used for the two types of measurements since electrophysiological recordings were conducted in vitro, but in both cases ecdysis was elicited by

and Truman (1984), we noted a large range in the average contraction periods, between 6 and 12 s at the beginning of the behavior to 12–20 s at the end. In our experiments most of the variability appeared to be a function of temperature: Video tracking at 21 °C resulted in initial periods of 6–7 s (Fig. 6a) and at 26 °C resulted in initial values of 12–13 s (Fig. 5b).

To the best of our knowledge, we have reported the first EMG recordings from larval muscles during ecdysis. Our EMG measurements were consistent with the larval-like patterns noted in transected adult preparations (Mesce and Truman 1988), although in general, the periods measured in larvae were longer (12–20 s) than those in the transected adults (5–10 s). The temperature at which the adult measurements were made in the prior work was not reported, and so whether the differences in the measured periods again can be explained by temperature differences or rather reflect developmental differences in the animals remains unclear.

Validity of use of ETH to initiate ecdysis

Using eclosion hormone (EH) and, more recently, ETH to initiate ecdysis has been a standard technique for many years (e.g., Weeks and Truman 1984; Ewer et al. 1997; Zitnan et al. 1996; Fig. 5). In particular, the ease of synthesizing ETH, compared to purification of EH from homogenized glands, has made it an extremely powerful tool for providing better control over the start time of the motor program. ETH works downstream of other initiators of ecdysis (e.g., Ecdysteroids and Corazonin: Truman and Weeks 1983; Zitnan et al. 1999; Kim et al. 2004), and yet it has never been determined whether ecdysis under these precocious (ETH-injected) conditions is similar to the naturally occurring behavior. We have shown, with our behavioral and EMG data, that ETH induces production of apparently normal ecdysis behaviors. This suggests that injected ETH is able to initiate the normal peptide cascade leading to ecdysis, albeit sooner relative to developmental timing, than that which would occur naturally.

Role of sensory feedback in ecdysis

Motor output in an intact animal can be very different from the fictive motor pattern produced by an isolated nervous system. For instance, significant differences have been measured in the frequencies and phasing between the motor patterns produced by intact and deafferented flying locusts (Wilson 1961; Pearson and Wolf 1987). In contrast, pyloric activity in crustacea is correlated directly with fictive activity from the stomatogastric nervous system in vitro (Marder and Bucher 2001). There are numerous examples of sensory feedback regulating aspects of ecdysis behaviors. Light was shown to be a trigger for initiation of

eclosion in *D. melanogaster* (McNabb et al. 1997). In *M. sexta*, activity from inhibitory neurons of the subesophageal ganglion was shown to control the timing of the onset of ecdysis, dictating when it started relative to pre-ecdysis, and removal of cuticle was observed to alter the duration of ecdysis (Weeks and Truman 1984; Zitnan and Adams 2000; Fuse and Truman 2002). In our experiments we noted the same ecdysis periodicity in whole animals (measured with video tracking or EMG) and in fictive motor programs from the isolated CNS when ecdysis was initiated with ETH (Fig. 6c). Moreover, the phase relationship between segments (Fig. 4a) appeared similar, and the decrease in frequency of contractions over time (Fig. 6c) was similar to that noted in the isolated CNS by other researchers (Weeks and Truman 1984; Gammie and Truman 1997). Thus, it appears that sensory feedback is not required to produce a physiologically relevant ecdysis motor pattern, nor is it responsible for the ecdysis rhythm slowing down over time. Our results contrast with the findings of a previous investigation in which the cycle period of fictive ecdysis motor patterns from a semi-intact deafferented nervous preparation stimulated with exogenous EH extracts was observed to be threefold longer than that for whole animal contractions (Weeks and Truman 1984). Whether this was due to temperature differences or a modulatory effect of EH is not clear.

We are currently extending our video tracking technique so that it can be used to analyze pre-ecdysis I and II behaviors. Our general approach could be readily applied to other animal systems involving complex movements and large data sets, as well. Automated analysis of large data sets produced in video tracking experiments will allow for greater phenotypic data mining and may lead to the identification of subtle differences in behaviors and even the discovery of complicated behavioral patterns that have not been previously identified (Vaughan et al. 2005).

# References

Albrecht DR, Bargmann CI (2011) High-content behavioral analysis of *Caenorhabditis elegans* in precise spatiotemporal chemical environments. Nature 8(7):599–606

Baek J-H, Cosman P, Feng Z, Silver J, Schafer WR (2002) Using machine vision to analyze and classify *Caenorhabditis elegans* behavioral phenotypes quantitatively. J Neurosci Methods 118(1):9–21

Balch T, Khan Z, Veloso M (2001) Automatically tracking and analyzing the behavior of live insect colonies. In: Proceedings of the 5th international conference on autonomous agents, pp 521–528

Bell RA, Joachim FG (1976) Techniques for rearing laboratory colonies of tobacco hornworms and pink bollworms. Ann Entomol Soc Am 69:365–373

Buckingham SD, Sattelle DB (2008) Strategies for automated analysis of *Caenorhabditis elegans* locomotion. Invert Neurosci 8:121–131

Copenhaver PF, Truman JW (1982) The role of eclosion hormone in the larval ecdyses of *Manduca sexta*. J Insect Physiol 28:695–701

Cronin CJ, Mendel JE, Mukhtar S, Kim YM, Stirbl RC, Bruck J, Sternberg PW (2005) An automated system for measuring parameters of nematode sinusoidal movement. BMC Genet 6:5

Dominick OS, Truman JW (1986) The physiology of wandering behaviour in *Manduca sexta*. iii Organization of wandering behaviour in the larval nervous system. J Exp Biol 121:115–132

Ewer J, Reynolds S (2000) Neuropeptide control of molting in insects. Hormones, brain and behavior, vol III. Elsevier Science, USA

Ewer J, Gammie SC, Truman JW (1997) Control of insect ecdysis by a positive-feedback endocrine system: roles of eclosion hormone and ecdysis triggering hormone. J Exp Biol 200:869–881

Fuse M, Truman JW (2002) Modulation of ecdysis in the moth, *Manduca sexta*; the roles of the suboesophageal and thoracic ganglia. J Exp Biol 205(8):1047–1058

Gammie SC, Truman JW (1997) Neuropeptide hierarchies and the activation of sequential motor behaviors in the hawkmoth, *Manduca sexta*. J Neurosci 17:4389–4397

Gammie SC, Truman JW (1999) Eclosion hormone provides a link between ecdysis-triggering hormone and crustacean cardioactive peptide in the neuroendocrine cascade that controls ecdysis behavior. J Exp Biol 202:343–352

Geng W, Cosman P, Berry CC, Feng Z, Schafer WR (2004) Automatic tracking, feature extraction and classification of *C. elegans* phenotypes. IEEE Trans Biomed Eng 51:1811–1820

Jain R, Kasturi R, Schunck BG (1995) Machine vision. McGraw Hill, New York

Kammer AE, Kinnamon SC (1977) Patterned muscle activity during eclosion in the hawkmoth, *Manduca sexta*. J Comp Physiol 114:313–326

Kim YJ, Spalovská-Valachová I, Cho KH, Adams ME, Zitnan D (2004) Corazonin receptor signaling in ecdysis initiation. PNAS USA 101(17):6704–6709

Lee H, Moody-Davis A, Saha U, Suzuki B, Asarnaw D, Chen S, Arkin M, Caffrey C, Singh R (2012) Quantification and clustering of phenotypic screening data using time series analysis for chemotherapy of schistosomiasis. BMC Genomics 13(Suppl 1):S4

Marcellino C, Gut J, Lim KC, Singh R, McKerrow J, Sakanari J (2012) WormAssay: a novel computer application for whole-plate screening of macroscopic parasites. PLoS Negl Trop Dis 6(1):e1494

Marder E, Bucher D (2001) Central pattern generators and the control of rhythmic movements. Curr Biol 11(23):R986–R996

McNabb SL, Baker JD, Agapite J, Steller H, Riddiford LM, Truman JW (1997) Disruption of a behavioral sequence by targeted death of peptidergic neurons in *Drosophila*. Neuron 19(4):813–823

Mesce KA, Truman JW (1988) Metamorphosis of the ecdysis motor pattern in the hawkmoth, *Manduca sexta*. J Comp Physiol A 163:287–299

Mezoff S, Papastathis N, Takesian A, Trimmer BA (2004) The biomechanical and neural control of hydrostatic limb movements in *Manduca sexta*. J Exp Biol 17:3043–3053

Novicki A, Weeks JC (1993) Organization of the larval pre-ecdysis motor pattern in the tobacco hornworm, *Manduca sexta*. J Comp Physiol [A] 173:151–162

Pearson KG, Wolf H (1987) Comparison of motor patterns in the intact and deafferented flight system of the locust. I. Electromyographic analysis. J Comp Physiol A 160:259–268

Schwartz LM, Truman JW (1983) Hormonal control of rates of metamorphic development in the tobacco hornworm *Manduca sexta*. Dev Biol 99:103–114

Shimoide A, Yoon I, Fuse M, Beale HC, Singh R (2005) Automated behavioral phenotype detection and analysis using color-based motion tracking. In: Proceedings of the 2nd Canadian conference on computer robot vision, IEEE Computer Society Press, pp 370–377

Singh R, Pittas M, Heskia I, Xu F, McKerrow JH, Caffrey C (2009) Automated image-based phenotypic screening for high-through-put drug discovery. In: Proceedings of the IEEE symposium on computer-based medical systems, IEEE Computer Society Press, pp 1–8

Swierczek NA, Giles AC, Rankin CH, Kerr RA (2011) High-throughput behavioral analysis in *C. elegans*. Nat Methods 8(7):592–598

Trimmer BA, Weeks JC (1989) Effects of nicotinic and muscarinic agents on an identified motoneurone and its direct afferent inputs in larval *Manduca sexta*. J Exp Biol 144:303–337

Truman JW, Weeks JC (1983) Hormonal control of the development and release of rhythmic ecdysis beahviours in insects. Symp Soc Exp Biol 37:223–231

Vaughan A, Singh R, Shimoide A, Yoon I, Fuse M (2005) Eigenphenotypes: towards an algorithmic framework for phenotype discovery. In: Proceedings of the IEEE computer systems bioinformatics conference, IEEE Computer Society Press, pp 77–78

Weeks JC, Truman JW (1984) Neural organization of peptide-activated ecdysis behaviors during the metamorphosis of *Manduca sexta*. I. Conservation of the peristalsis motor pattern at the larval-pupal transformation. J Comp Physiol A 155:407–422

Wells C, Aparicio K, Salmon A, Zadel A, Fuse M (2006) Structure-activity relationship of ETH during ecdysis in the tobacco hornworm, *Manduca sexta*. Peptides 27(4):698–709

Wilson DM (1961) The central nervous control of flight in a locust. J Exp Biol 38:471–490

Zitnan D, Adams ME (2000) Excitatory and inhibitory roles of central ganglia in initiation of the insect ecdysis behavioural sequence. J Exp Biol 203:1329–1340

Zitnan D, Kingan TG, Hermesman JL, Adams ME (1996) Identification of ecdysis-triggering hormone from an epitracheal endocrine system. Science 271:88–91

Zitnan D, Ross LS, Zitnanova I, Hermesman JL, Gill SS, Adams ME (1999) Steroid induction of a peptide hormone gene leads to orchestration of a defined behavioral sequence. Neuron 23:523–535